

Supporting Information

Phase Transformations in TiS₂ during K Intercalation

Bingbing Tian^{†,‡,#}, Wei Tang^{§,#}, Kai Leng^{‡,#}, Zhongxin Chen[‡], Sherman Jun Rong Tan[‡], Chengxin Peng[‡], Guo-Hong Ning[‡], Wei Fu[‡], Chenliang Su^{†,‡}, Guangyuan Wesley Zheng[§], Kian Ping Loh^{*†,‡}

[†] *International Collaborative Laboratory of 2D Materials for Optoelectronics Science and Technology, Key Laboratory of Optoelectronic Devices and Systems of Ministry of Education and Guangdong Province, College of Optoelectronic Engineering, Shenzhen University, Shenzhen 518060, China.*

[‡] *Department of Chemistry, Centre for Advanced 2D Materials (CA2DM) and Graphene Research Centre, National University of Singapore, 3 Science Drive 3, Singapore 117543, Singapore.*

[§] *Institute of Materials Research and Engineering, A*STAR, 2 Fusionopolis Way, Innovis, Singapore 138634, Singapore.*

* Corresponding Authors: Kian Ping Loh, Email: chmlohkp@nus.edu.sg

MATERIALS AND METHODS

Electrodes preparation and electrochemical analysis

Single crystal TiS_2 powder was purchased from 2D AGE. The electrodes were fabricated using the following procedure. The TiS_2 , Super P and polyvinylidene fluoride (PVDF) binder were mixed in a ratio of 80:10:10 in the N-methyl-2-pyrrolidone (NMP) to form a well-dispersed slurry by stirring overnight and then coated onto a Carbon Paper substrate (AvCarb GDS2120, Fuel Cell Etc). Coatings were dried immediately in a blast oven at 50 °C for about 2 h, followed by activation in a vacuum oven at 50 °C for 24 h to produce membranes that were then cut into circular electrode discs with a diameter of 14 mm for later use.

After weighing the electrode discs (active material loading: 6-8 mg cm^{-2}), the cells were assembled in a glovebox (VAC) under Ar atmosphere with H_2O and O_2 contents lower than 1 ppm, using CR2016 coin cell hardware, with lithium, sodium and potassium metals as the counter electrodes and Whatman Glass Microfibre Filter as separator. The electrolyte for Li-ion batteries testing was a commercial one of 1 M LiPF_6 in a mixture of ethylene carbonate (EC) and diethyl carbonate (DEC) (1:1 vol.%). The electrolyte for Na-ion batteries was 0.8 M NaPF_6 in a mixture of ethylene carbonate (EC) and diethyl carbonate (DEC) (1:1 vol.%). The electrolyte for K-ion batteries was 0.8 M KPF_6 in a mixture of ethylene carbonate (EC) and diethyl carbonate (DEC) (1:1 vol.%).

Cyclic voltammetry (CV) was performed using an Ivium-n-Stat multi-channel electrochemical analyser. Cyclic voltammograms were recorded over the potential range of 1.5-3.0 V, 1.2-2.7 V and 1.0-3.0 V for Li-, Na- and K-ion batteries, respectively, at a scanning rate of 0.1 mV s^{-1} , starting from OCP into the cathodic scan (discharge) direction. Galvanostatic discharge-charge cycling of the batteries was monitored within the voltage window of 1.5-3.0 V, 1.2-2.7 V and 1.0-3.0 V for Li-, Na- and K-ion batteries, respectively, using a LAND Battery Tester. The potentials hereafter are given versus Li/Li^+ for Li-ion batteries, Na/Na^+ for Na-ion batteries, K/K^+ for K-ion batteries. All the Electrochemical measurements were performed at room temperature.

Chemical pre-potassiation procedure and fabrication of $\text{K}_{0.25}\text{TiS}_2$ electrodes

The chemical pre-potassiation of the single crystal TiS_2 powder was carried out with a potassium naphthalenide treating process in THF solution in a glovebox.¹ After reaction, washing, centrifugation and drying in glovebox, K_xTiS_2 powder obtained. As it is rather difficult to control the potassium content during K^+ chemical intercalation, the electrochemical specific capacity is used to accurately determine the potassium content of an as-synthesized K_xTiS_2 .

The $\text{K}_{0.25}\text{TiS}_2$ electrodes fabrication process is similar to that of preparing single crystal TiS_2 electrodes, except all the procedures are performed in a glovebox. The slurry was uniformly scraped on Al foil with a blade, and subsequently the electrodes were vacuum-dried at $70 \text{ }^\circ\text{C}$ in the antechamber of the glovebox. After weighing, the

active material loading in the electrode discs was about 3 mg cm^{-2} . Then the as-prepared electrodes are used for CR2016-type coin cells.

***In-situ* XRD measurement, TEM and electrochemistry**

Complimentary to these techniques, *in-situ* XRD experiments recorded on a BRUKER D8 diffractometer with a Cu K α X-ray source, were performed by utilizing an electrochemical cell capped by a beryllium window functioning as the positive current collector. A detailed description of the cell can be found elsewhere.² Transmission electron microscopy (TEM) analysis was performed on an FEI Titan 80-300 S/TEM (Scanning Transmission Electron Microscope) operated at 200 kV. The electrochemistry of this cell was controlled by a LAND Battery Tester, at a discharge rate of c.a. 0.1 C (24 mA g⁻¹, discharge or charge in about 10 h) and XRD patterns were collected at intervals of 10 min.

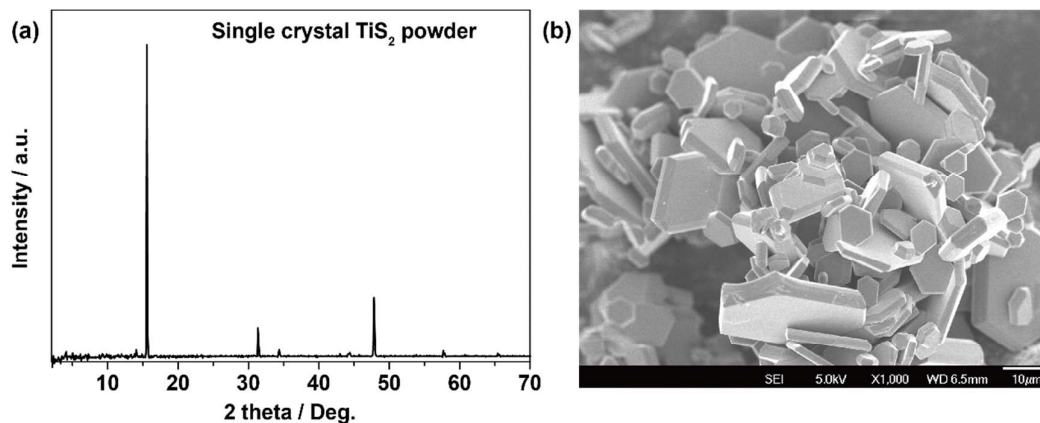


Figure S1. (a) The XRD pattern of single crystal TiS_2 powder. The TiS_2 powders have the hexagonal structure matching JCPDS No. 88-1967 and show only the TiS_2 phase, without any impurities; (b) SEM image of single crystal TiS_2 powder. The single crystal TiS_2 powder shows a platelet morphology.

Owing to preferred orientation of single crystal TiS_2 , the peak intensity of TiS_2 electrode in the *in-situ* cell is quite weak except the (001) peak, so Rietveld analysis could not be readily carried out. However, for the layered TiS_2 material, the main structure evolution can be obtained through interlayer spacing changing during the charge/discharge process. In this work, only the (001) intense peak was used to extract the c lattice parameters that corresponds to the interlayer spacing.

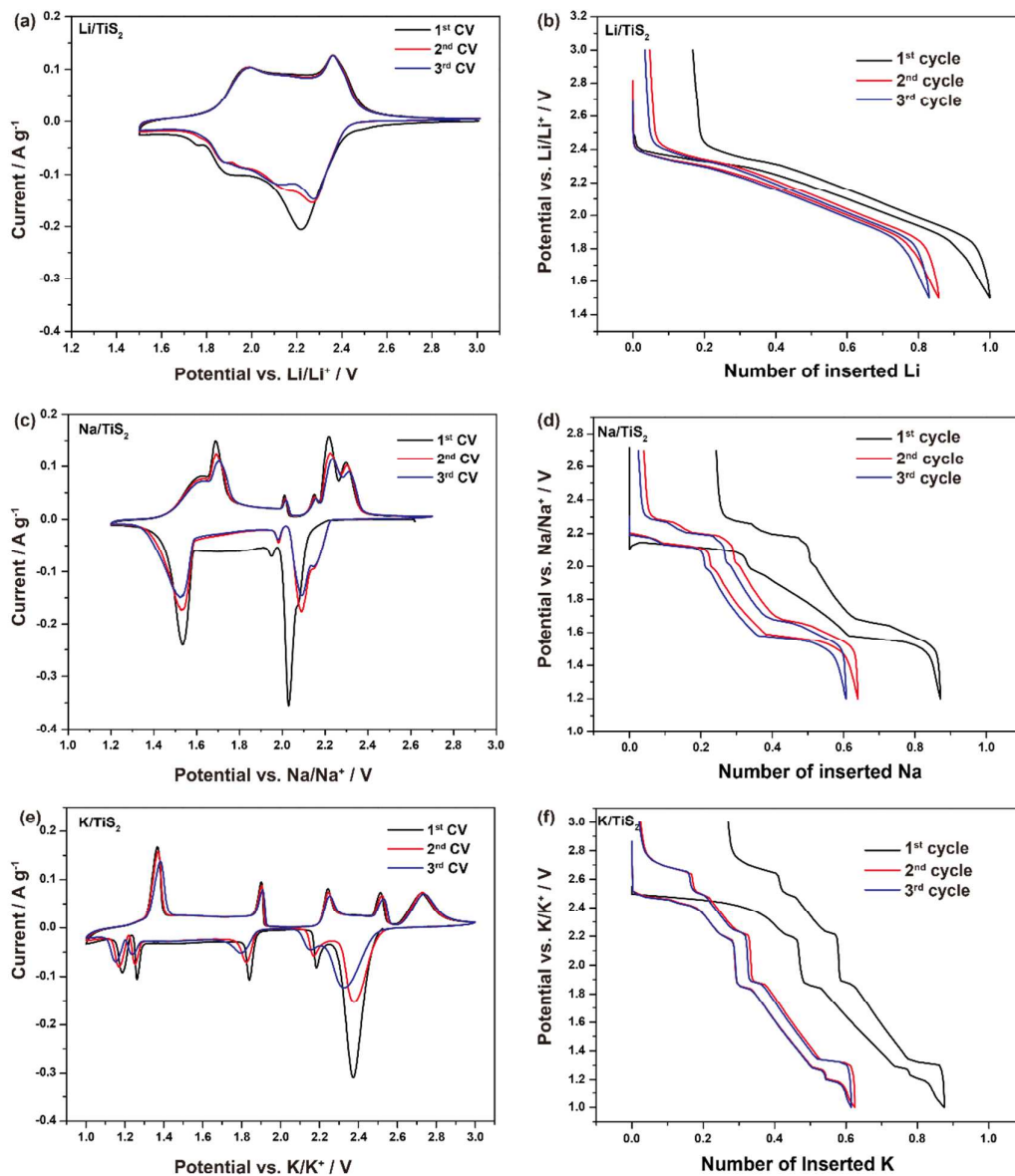


Figure S2. Electrochemical behaviors of TiS₂ electrodes for Li-ion, Na-ion and K-ion batteries. (a), (c) and (e) the first three CV curves of bulk TiS₂ electrode at a scan rate of 0.1 mV s⁻¹; (b), (d) and (f) discharge/charge profiles of bulk TiS₂ electrode at a current rate of 0.1 C (1C=240 mA g⁻¹) in the voltage range of 1.5 to 3.0 V versus Li/Li⁺, 1.2 to 2.7 V versus Na/Na⁺ and 1.0 to 3.0 V versus K/K⁺, respectively.

The first three cyclic voltammograms (CVs) and galvanostatic discharge/charge profiles in K/TiS₂ cells are shown in **Figure S2 (e, f)** to evaluate the electrochemical behaviors of the TiS₂ electrodes for KIBs. In the CVs of a K/TiS₂ cell, five cathodic peaks (located at 2.37, 2.19, 1.84, 1.26 and 1.19 V) and five anodic peaks (located at 2.73, 2.51, 2.25, 1.90 and 1.36 V) are observed, indicating that continuous multiphase changes occur during the potassiation/depotassiation processes. Plateaus at similar potentials, consistent with CVs, are also observed in the discharge and charge profiles. The initial potassiation discharge capacity of the TiS₂ electrode is 210.7 mA h g⁻¹ when discharged to 1.0 V, corresponding to 0.88 mole of K⁺ intercalated into 1 mole TiS₂ forming K_{0.88}TiS₂. The following depotassiation charge capacity is only 145.8 mA h g⁻¹, with a low initial coulombic efficiency of 69.2%. The second discharge/charge capacities are 150.4 and 144.5 mA h g⁻¹, respectively, with a coulombic efficiency higher than 96%. Comparing the initial and second discharge profiles, the capacity loss mainly exists in the plateau of 2.5-2.3 V, which is consistent with the intensity decrease of the first cathode peak (C₁) in the second CVs. This partially irreversible potassiation/depotassiation process is responsible for the low coulombic efficiency in the first cycle. As determined from the loss capacity (64.9 mA h g⁻¹) of the first discharge to charge, about 0.25 eq. K is deactivated in TiS₂ (formed K_{0.25}TiS₂) after the first cycle. We associate this recurring deactivation behavior in the first discharge/charge cycle to the energy loss expended during the formation of an intermediate phase, which is elaborated in later sections. This

provides a potential avenue for improving coulombic efficiency and cycling performance of TiS_2 for KIBs.

For comparison, the CVs and discharge/charge profiles of TiS_2 electrodes for Li-ion and Na-ion batteries are also evaluated and shown here. In the Li/ TiS_2 cell, two pairs of broad peaks centered at 2.3 and 1.95 V are observed in CV curves. A slope with an obvious plateau at about 2.3 V is present in the discharge curve, in agreement with the CV data. However, one pair of peaks centered at 1.95 V is not seen in the discharge/charge curves due to the superior kinetic properties of TiS_2 during Li insertion.³ For the Na/ TiS_2 cell, two sharp cathodic peaks located at 2.0 and 1.5 V are observed in CV curves. In the anodic process, one sharp peak (1.7 V) with a shoulder (1.6 V) and a series anodic peaks at 2.0, 2.15, 2.22 and 2.30 V are observed, indicating a reversible reaction process of multiphase coexistence. At the first discharge, the Na/ TiS_2 cell shows a discharge capacity of $\sim 230 \text{ mA h g}^{-1}$ corresponding to the movement of ~ 0.96 Na ions per TiS_2 . During the discharging process, two plateaus occur at the potentials of 2.1 V and 1.6 V, which is similar to the previous reports¹ and also in agreement with the CV data. The peaks in the CV curves and plateaus in the discharge and charge profiles maintain well in the second and third cycles.

In-situ XRD results

Li/TiS₂ cell

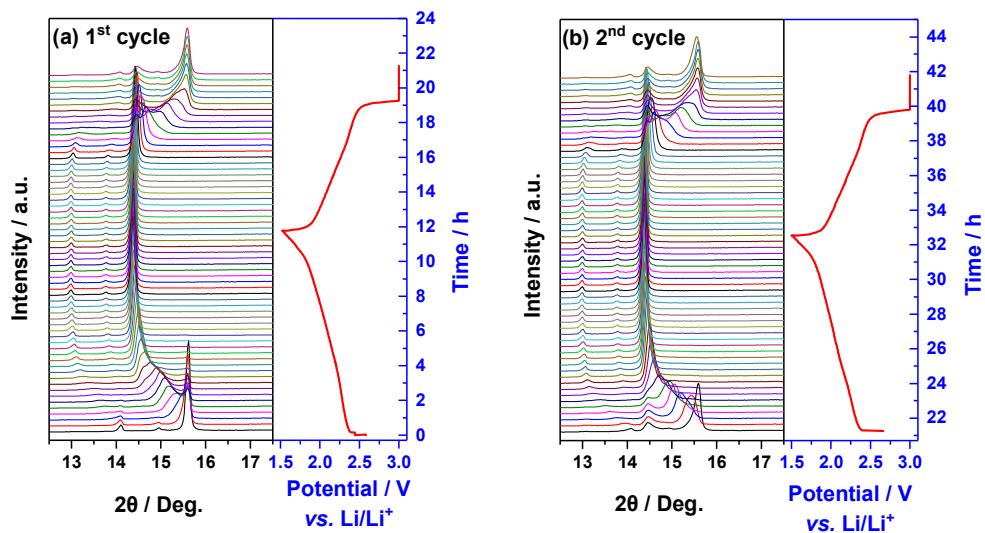


Figure S3. Structural evolution during lithiation and delithiation. *In-situ* XRD patterns collected during the first and second discharge/charge of the Li/TiS₂ cell under a current rate of 0.1 C at the voltage range between 1.5 and 3.0 V. (a) Structural evolution in the first cycle; (b) Structural evolution in the second cycle.

Na/TiS₂ cell

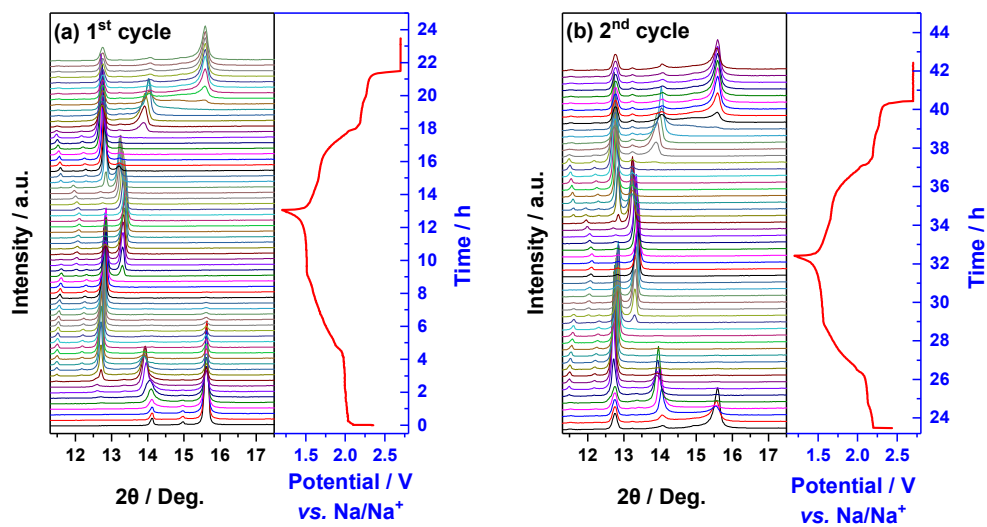


Figure S4. Structural evolution during sodiation and desodiation. *In-situ XRD* patterns collected during the first and second discharge/charge of the Na/TiS₂ cell under a current rate of 0.1 C at the voltage range between 1.2 and 2.7 V. (a) Structural evolution in the first cycle; (b) Structural evolution in the second cycle.

K/TiS₂ cell

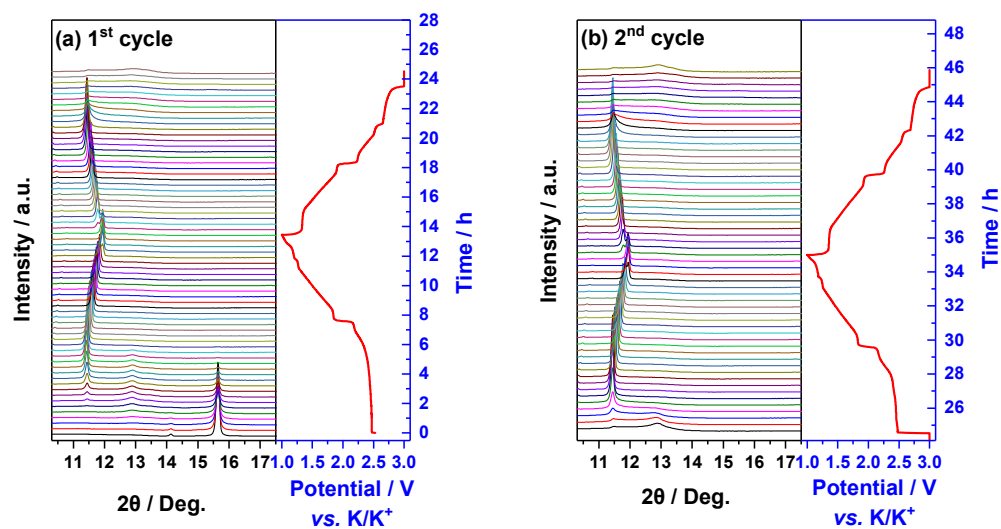


Figure S5. Structural evolution during potassiation and depotassiation. *In-situ XRD* patterns collected during the first and second discharge/charge of the K/TiS₂ cell under a current rate of 0.1 C at the voltage range between 1.0 and 3.0 V. (a) Structural evolution in the first cycle; (b) Structural evolution in the second cycle.

Numerous studies on Li intercalation into TiS_2 have been implemented to reveal the phase transformations during electrochemical process.⁴⁻⁷ A two phase reaction occurs during the lithiation and delithiation process, with a solid-solution process between the two phases of TiS_2 and LiTiS_2 . The phase evolution is also in good agreement with the *in-situ* XRD results exploited herein (Figure S3). From the *in-situ* XRD results of the Na/TiS_2 cell (Figure S4), a stage 4^{Na} phase was discovered in addition to the known stage 1, 2^{Na} and 3^{Na} phases.^{8 - 11} Four types of three-dimensionally ordered superstructures were observed: For $x < 0.25$, phase 1 change to phase 2^{Na} ; For $0.25 < x < 0.75$ exclusively the rather complicated pattern is found; For $0.75 < x < 0.96$, phase 3^{Na} transfer to phase 4^{Na} . When charged, reversible phase transformations are observed with partially irreversible capacity (coulomb efficiency: ~84%).

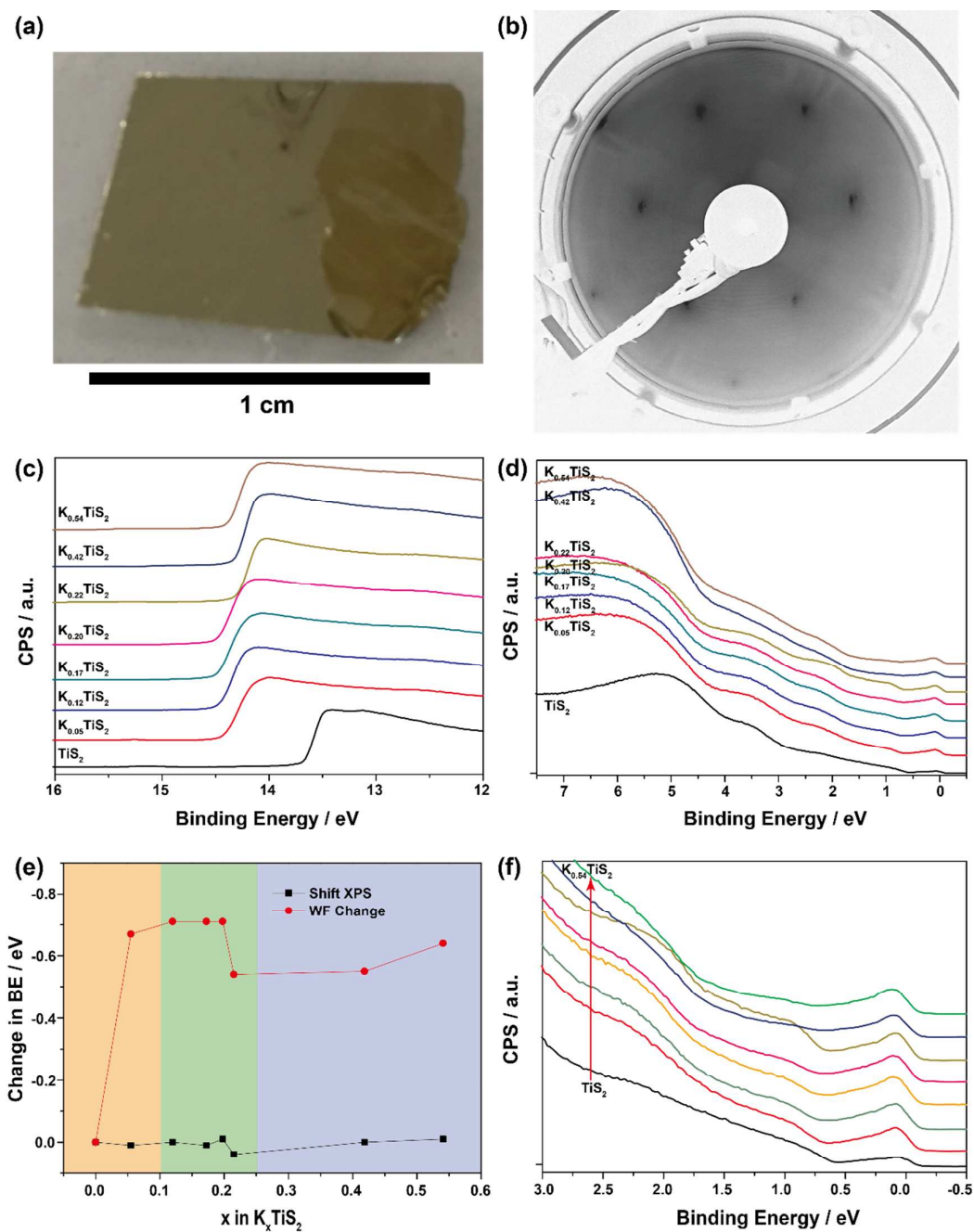


Figure S6. UPS experiment for the single crystal TiS_2 ($\sim 1 \times 1 \text{ cm}^2$). (a) Photo image of single crystal TiS_2 purchased from HQ Graphene; (b) Low energy electron diffraction (LEED) image of the TiS_2 single crystal taken at 179V; (c) UPS spectra in the secondary electron cut-off (SECO) region with an applied bias of -3V to the sample;

(d) UPS spectra in the low binding energy region (valence band region); (e) Work function (WF) change and XPS binding energy shift of the Ti 2p core level with the content of K in TiS_2 (K_xTiS_2); (f) Enlargement of UPS spectra in lower binding energy region.

The work function of the sample can be extracted using the formula $\text{WF} = h\nu - \text{BE}$ where $h\nu$ is photon energy of He I of 21.218 eV, and BE can be determined by the SECO after a subtraction of -3V from the added bias.

In-situ potassium deposition on single crystal TiS_2 flake is performed in an UHV system directly connected with an UPS. Its properties for K insertion are evaluated by UPS and XPS. In the early stage of the deposition ($x < 0.22$), K intercalates into TiS_2 spontaneously. Subsequently, thermal activation is needed to insert a higher concentration of K. This suggests the possibility of a new TiS_2 phase. The energy pathway for K^+ diffusion lies along the c-axis channel in the (001) direction. As the concentration of potassium increases in TiS_2 structure, the work function (WF) (Figure S6) decreases sharply, indicative of vacuum level lowering due to formation of interface dipole. The vacuum level remains constant with increasing K content until $x \approx 0.25$, where the vacuum level is increased again. This implies that the charge transfer between K and TiS_2 decreases possibly due to the formation of a different phase. Phase transformation can be also deduced by monitoring the binding energy change in the Ti 2p peak. At the early stages of K intercalation, there is no XPS shift since both K and TiS_2 are metals, there is no observed band bending associated with adsorption. With K intercalation, the charge transfer between K and TiS_2 is

insufficient to shift the Ti 2p core energy levels due to the high concentration of electrons in the metallic TiS₂. Consistent with the vacuum level increase at $x \approx 0.25$ of K, we observed a sudden increase in XPS binding energies. Following our phase restructuring model,¹² the increases edge density would allow increased electron transfer from the K to TiS₂, which leads to the increase in Ti 2p core level binding energy shift due to the migration of Fermi level towards the conduction band. The sharp change in WF and XPS peak binding energies in addition to the thermal activation required for further K intercalation when $x \approx 0.25$ supports phase transformation observed in our *in-situ* XRD study.

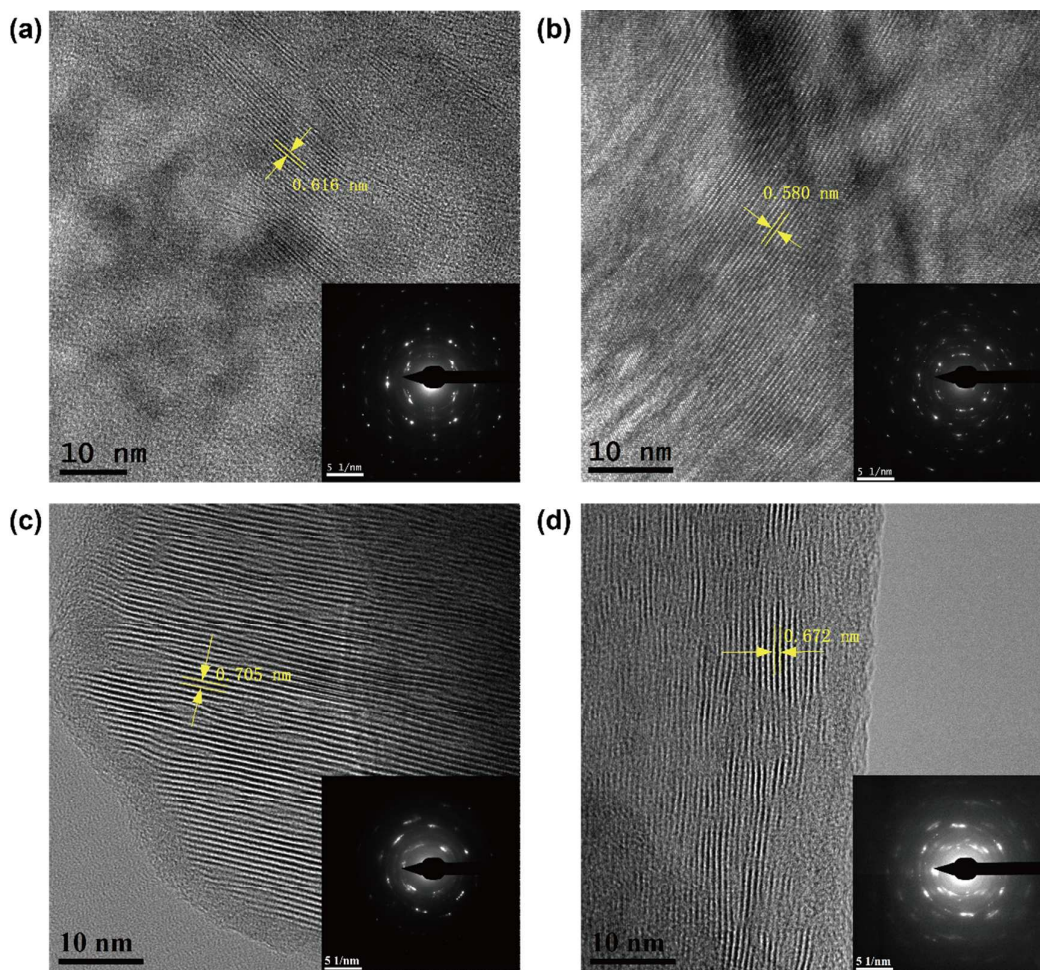


Figure S7. HRTEM images (a, b, c, d) and SAED patterns (a inset, b inset, c inset, d inset) of TiS_2 electrodes during lithiation and delithiation, sodiation and desodiation. The TiS_2 electrodes (a) lithiation (discharged to 1.5 V in the first cycle) and (b) delithiation (recharged to 3.0 V in the first cycle); The TiS_2 electrodes (c) sodiation (discharged to 1.2 V in the first cycle) and (d) desodiation (recharged to 2.7 V in the first cycle).

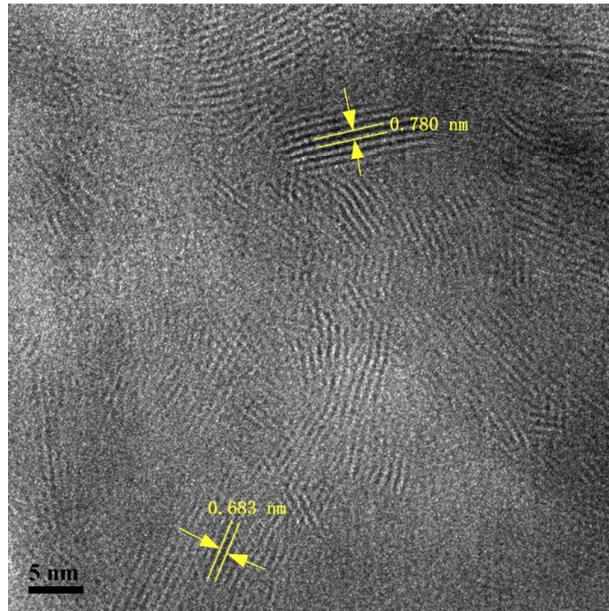


Figure S8. Lattice resolution HRTEM image of the $K_{0.25}TiS_2$ sample (large scale).

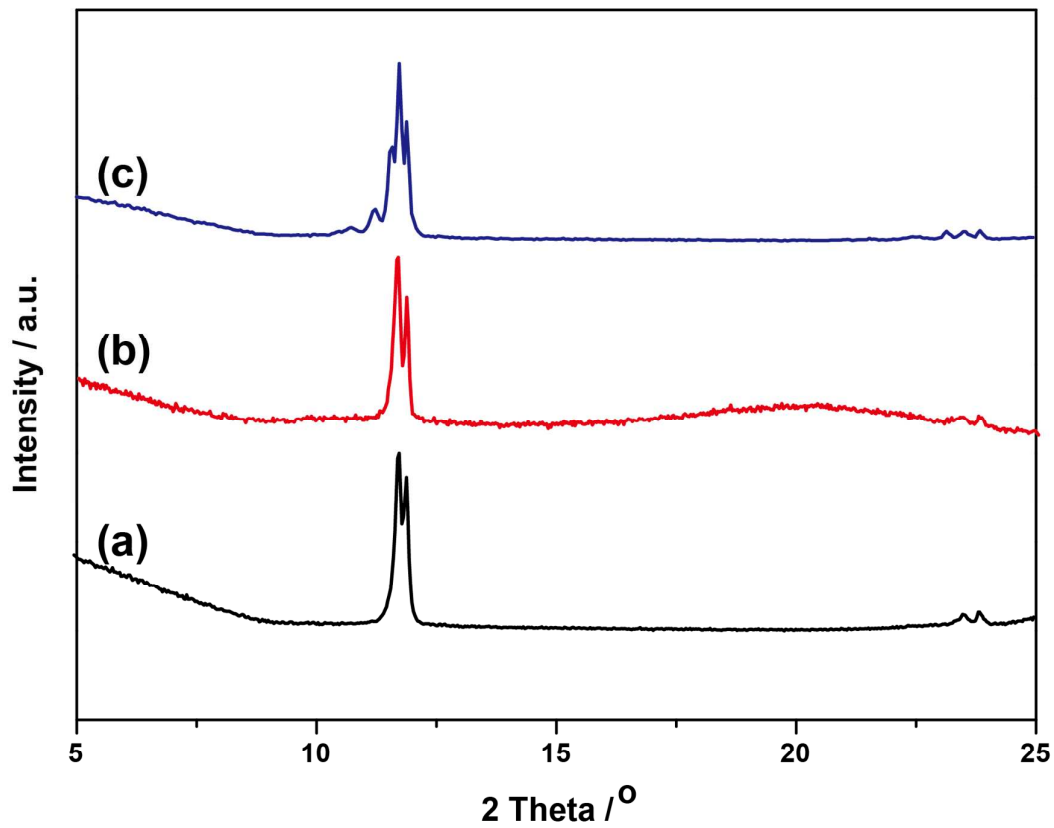


Figure S9. XRD patterns of the chemical pre-potassiated TiS₂ at different pre-potassiation time and concentration of potassium naphthalenide solution. The conditions for treating pristine TiS₂: ratio and time of K:Naphthalene:TiS₂ are (a)1.5:1.5:1, for 8h; (b)2:1:1, for 36h; (c)3:1.5:1, for 48h.

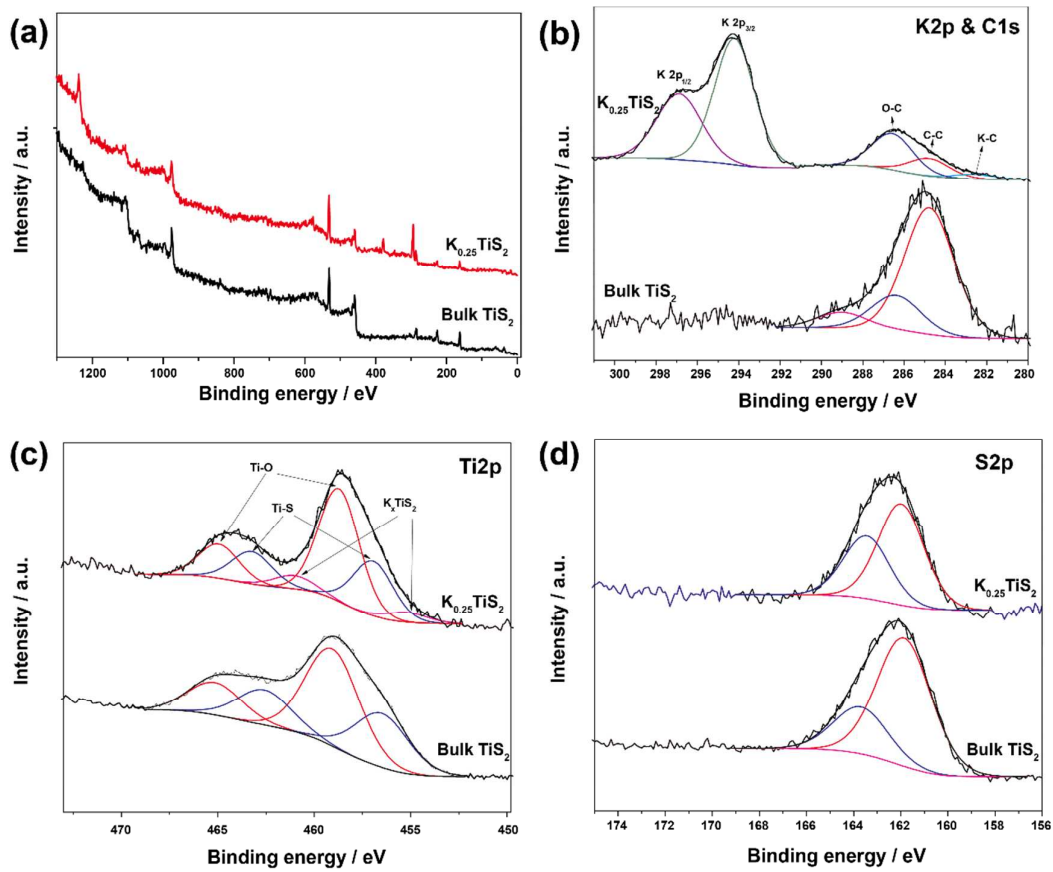


Figure S10. XPS (a) survey spectra, (b) K2p & C1s, (c) Ti2p, (c) S2p core level spectra of the bulk TiS_2 and the $\text{K}_{0.25}\text{TiS}_2$.

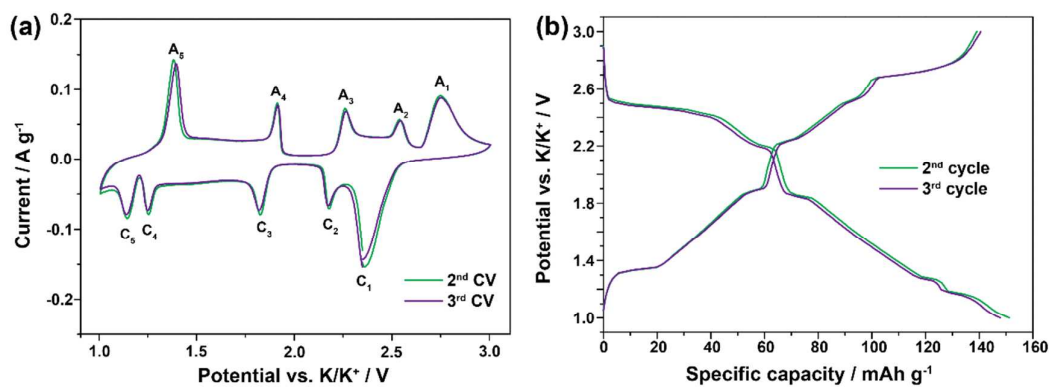


Figure S11. Electrochemical behaviors of the chemically pre-potassiated TiS₂ electrodes (K_{0.25}TiS₂) of the second and third cycles: (a) CV curves at a scan rate of 0.1 mV s⁻¹; (b) discharge/charge profiles at a current rate of 0.1 C (24 mA g⁻¹) in the voltage range of 1.0 to 3.0 V versus K/K⁺.

References

- (1) Zheng, J.; Zhang, H.; Dong, S.; Liu, Y.; Nai, C. T.; Shin H. S.; Loh, K. P. High Yield Exfoliation of Two-Dimensional Chalcogenides Using Sodium Naphthalenide. *Nat. Commun.* **2014**, *5*, 2995.
- (2) Leriche, J. B.; Hamelet, S.; Shu, J.; Morcrette, M.; Masquelier, C.; Ouvrard, G.; Zerrouki, M.; Soudan, P.; Belin, S.; Elkaïm E.; Baudalet, F. An Electrochemical Cell for *Operando* Study of Lithium Batteries Using Synchrotron Radiation. *J. Electrochem. Soc.* **2010**, *157*, A606-A610.
- (3) Whittingham, M. S. Electrical Energy Storage and Intercalation Chemistry. *Science* **1976**, *192*, 1126-1127.
- (4) Silbernagel B. G.; Whittingham, M. S. An NMR Study of the Alkali Metal Intercalation Phase Li_xTiS_2 : Relation to Structure, Thermodynamics, and Ionicity. *J. Chem. Phys.* **1976**, *64*, 3670-3673.
- (5) Whittingham, M. S. Chemistry of Intercalation Compounds: Metal Guests in Chalcogenide Hosts. *Prog. Solid St. Chem.* **1978**, *12*, 41-99.
- (6) Elazari, R.; Salitra, G.; Gershinshy, G.; Garsuch, A.; Panchenko A.; Aurbach, D. Li Ion Cells Comprising Lithiated Columnar Silicon Film Anodes, TiS_2 Cathodes and Fluoroethylene Carbonate (FEC) as a Critically Important Component. *J. Electrochem. Soc.* **2012**, *159*, A1440-A1445.
- (7) Unemoto, A.; Ikeshoji, T.; Yasaku, S.; Matsuo, M.; Stavila, V.; Udovic T. J.; Orimo, S. Stable Interface Formation between TiS_2 and LiBH_4 in Bulk-Type All Solid-State Lithium Batteries. *Chem. Mater.* **2015**, *27*, 5407-5416.

-
- (8) Silbernagel B. G.; Whittingham, M. S. The Physical Properties of the Na_xTiS_2 Intercalation Compounds: A Synthetic and NMR Study. *Mat. Res. Bull.* **1976**, *11*, 29-36.
- (9) Newman G. H.; Klemann, L. P. Ambient Temperature Cycling of an Na-TiS₂ Cell. *J. Electrochem. Soc.* **1980**, *127*, 2097-2099.
- (10) Molinie, P.; Trichet, L.; Rouxel, J.; Berthier, C.; Chabre Y.; Segransan, P. The Na-TiS₂ System: A Critical Discussion of the Phase Boundaries, Structural and NMR Studies. *J. Phys. Chem. Solids* **1984**, *45*, 105-112.
- (11) Ryu, H.-S.; Kim, J.-S.; Park, J.-S.; Park, J.-W.; Kim, K.-W.; Ahn, J.-H.; Nam, T.-H.; Wang G.; Ahn, H.-J. Electrochemical Properties and Discharge Mechanism of Na/TiS₂ Cells with Liquid Electrolyte at Room Temperature. *J. Electrochem. Soc.* **2013**, *160*, A338-A343.
- (12) Tan, S. J. R.; Abdelwahab, I.; Ding, Z.; Zhao, X.; Yang, T.; Loke, G. Z. J.; Lin, H.; Verzhbitskiy, I.; Poh, S. M.; Xu, H.; Nai, C. T.; Zhou, W.; Eda, G.; Jia B.; Loh, K. P. Chemical Stabilization of 1T' Phase Transition Metal Dichalcogenides with Giant Optical Kerr Nonlinearity. *J. Am. Chem. Soc.* **2017**, *139*, 2504-2511.